Hydrol. Earth Syst. Sci. Discuss., 9, 1207–1249, 2012
www.hydrol-earth-syst-sci-discuss.net/9/1207/2012/
doi:10.5194/hessd-9-1207-2012

Hydrology and Earth System Sciences Discussions

Modifying a dynamic global vegetation model for simulating large spatial scale land surface water balance

G. Tang[1,2] **and P. J. Bartlein**[1]

[1]Department of Geography, University of Oregon, Eugene, OR 97403, USA
[2]Division of Earth and Ecosystem Sciences, Desert Research Institute, Reno, NV 89512, USA

Received: 13 November 2011 – Accepted: 20 November 2011 – Published: 23 January 2012

Correspondence to: G. Tang (tangg2010@gmail.com)

Published by Copernicus Publications on behalf of the European Geosciences Union.

Abstract

Water balance models of simple structure are easier to grasp and more clearly connect cause and effect than models of complex structure. Such models are essential for studying large spatial scale land surface water balance in the context of climate and land cover change, both natural and anthropogenic. This study aims to (i) develop a large spatial scale water balance model by modifying a dynamic global vegetation model (DGVM), and (ii) test the model's performance in simulating actual evapotranspiration (ET), soil moisture and surface runoff for the coterminous United States (US). Toward these ends, we first introduced development of the "LPJ-Hydrology" (LH) model by incorporating satellite-based land covers into the Lund-Potsdam-Jena (LPJ) DGVM instead of dynamically simulating them. We then ran LH using historical (1982–2006) climate data and satellite-based land covers at 2.5 arc-min grid cells. The simulated ET, soil moisture and surface runoff were compared to existing sets of observed or simulated data for the US. The results indicated that LH captures well the variation of monthly actual ET ($R^2 = 0.61$, $p < 0.01$) in the Everglades of Florida over the years 1996–2001. The modeled monthly soil moisture for Illinois of the US agrees well ($R^2 = 0.79$, $p < 0.01$) with the observed over the years 1984–2001. The modeled monthly stream flow for most 12 major rivers in the US is consistent ($R^2 > 0.46$, $p < 0.01$; Nash-Sutcliffe Coefficients >0.52) with observed values over the years 1982–2006, respectively. The modeled spatial patterns of annual ET and surface runoff are in accordance with previously published data. Compared to its predecessor, LH simulates better monthly stream flow in winter and early spring by incorporating effects of solar radiation on snowmelt. Overall, this study proves the feasibility of incorporating satellite-based land-covers into a DGVM for simulating large spatial scale land surface water balance. LH developed in this study should be a useful tool for studying effects of climate and land cover change on land surface hydrology at large spatial scales.

HESSD

9, 1207–1249, 2012

1 Introduction

Evapotranspiration (ET), soil moisture and surface runoff are three major components of the hydrologic cycle at the land surface and affect many important processes in the soil-vegetation-atmosphere system (Lu et al., 2003; Murphy and Lodge, 2004). For example, changes in actual and potential ET have implications for nutrient flux, forest function and plant productivity (e.g. Kosugi and Katsuyama, 2007), and for the global carbon cycle (Engstrom et al., 2006). Soil moisture can influence near-surface atmospheric variability (Arora and Boer, 2006) and atmospheric circulation on seasonal-to-interannual time scales (Shukla and Mintz, 1982; Manabe and Delworth, 1990). Soil-moisture deficits can also restrict the respiration and productivity of plants and thus influence species composition, type and structure of vegetation (Brabson et al., 2005; Evans and Trevisan, 1995). Shifts in surface runoff influence the ability of regional water supply and demand and the cycling of nutrients on the globe. The importance of ET, soil moisture and surface runoff for human well-being, terrestrial ecosystems and agricultural sustainability requires that we be able to simulate the water balance at the land surface.

Dynamic global vegetation models (DGVM), such as the Lund-Potsdam-Jena (LPJ) DGVM (Stich et al., 2003; Gerten et al., 2004) that has its own hydrologic model, have illustrated strong ability to simulate land surface water balance at regional to global scales. This ability, however, might not be accessible to users who have strong interest in land surface water balance because (i) DGVMs mainly address the biogeographic (e.g., species distribution) and biogeochemical (e.g., carbon flux) dynamics of terrestrial ecosystems. Using DGVMs to simulate the land surface water balance requires users to define and parameterize the bioclimatic, biogeochemical and physiological attributes of plants, which can be challenging; (ii) DGVMs often require the spin-up simulation for hundreds of years (e.g., 1000 yr) to have vegetation and soil carbon to reach an equilibrium state with long-term climate (e.g., Hickler et al., 2004). The running of model can be time-consuming for large spatial scale study while at fine resolution; and (iii) the limitations of DGVMs (e.g., exclusion of seed dispersal) may

HESSD
9, 1207–1249, 2012

cause themselves to fail to simulate vegetation at local scale, which in turn affects the accuracy of modeled land surface water balance.

Nevertheless, DGVMs integrate roles of climate variation, vegetation, soil features and atmospheric composition (i.e., CO_2) in controlling ET, soil moisture and runoff at the land surface. These advantages should be accessible to users who are not ecologists but of strong interest in modeling land surface hydrology at large spatial scale. Given the complexity of DGVMs, incorporating static land covers into DGVMs, instead of simulating them, is a way to achieve this end. For the purpose of simulating the land surface hydrology, such incorporation will (i) simplify model's structure by making representations of some mechanistic processes like plant growth and soil heterotrophic respiration unnecessary; (ii) reduce the task of model's parameterization associated with plant bioclimatic, biogeochemical and physiological attributes; (iii) increase model's computing efficiency by avoiding the "spin-up" simulation; and (iv) contribute to the accuracy of model simulation because satellite-based land covers are often thought of high accuracy in representing the land characteristics. In fact, satellite-based data have been widely used in modeling the land surface water balance (e.g., Glenn et al., 2007; Song et al., 2000).

The goals of this study are to (i) present an attempt to modify LPJ-DGVM (Sitch et al., 2003; Gerten et al., 2004) for the purpose of simulating large spatial scale land surface water balance under predefined land covers, and (ii) test the application of this model, named LH (LPJ-hydrology), in coterminous United States (US). Toward these ends, we first introduce development of the LH model and the parameterization of some key hydrologic variables in LH. We then run LH at 2.5 arc-min land grids using historical climate data for the period 1982–2006 and satellite-based land covers. The simulated ET, soil moisture and surface runoff are tested against existing sets of observed or simulated data using different methods, including LH's predecessor. With this study, we not only test the feasibility of incorporating static land covers into a DGVM for simulating large spatial scale land surface water balance but also provide an efficient tool for studying effects of climate and land cover change on land surface hydrology.

HESSD
9, 1207–1249, 2012

2 Methods and data

2.1 The development of LH model

The large spatial scale stand-alone LH (LPJ-hydrology) model was developed by modifying LPJ-DGVM (Stich et al., 2003; Gerten et al., 2004) and shares many of its features. In general, LH consists of three main sub-models: (i) the potential ET model that calculates pseudo-daily photosynthetic active radiation flux, day length and daily equilibirum potential ET in each grid cell using input climate data with latitude information; (ii) the summer phenology model that evaluates daily leaf phenology of predefined land covers; and (iii) the water balance model coupled with plant photosynthesis that simulates major components of water balance among the soil, vegetation and the atmosphere, including soil evaporation, plant transpiration, soil moisture and surface runoff (Fig. 1).

The input land cover data in LH is used to (i) initialize some hydrologic and photosynthetic relevant parameters (Tables 1 and 2), (ii) define the phenological features of each predefined land cover as one of four types, i.e., evergreen, summergreen, raingreen and other, and (iii) specify the photosynthetic pathway of plants (i.e., C4 vs. C3). The foliar vegetative cover is used to calculate plant-specific minimum canopy conductance and the total amount of interception loss of precipitation by plants. In this study, we define land covers in the coterminous US into 11 types based on the global land cover classification data (Hansen et al., 2000), of which five types are forests (two evergreen, two deciduous and one mixed) and six are non-forest (one woodland, one shrub land, one grassland, one cropland, one bare and one urban) (Table 1). For each land cover, the percentage of foliar vegetative cover varies from 0 to 100 percent.

In addition to vegetation-related data, other data needed to run LH include monthly mean values of temperature (°C), precipitation (mm), wet-day frequency (days) and percent cloudiness or sunshine (%), and atmospheric CO_2 concentration. The CO_2 data are used to calculate non-water-stressed canopy conductance and intercellular CO_2 partial pressure (Haxeltine and Prentice, 1996). The soil data used in LH still

HESSD
9, 1207–1249, 2012

consists of two layers with fixed thickness (upper, 50 cm; lower, 100 cm). To better initialize some important variables such as soil moisture content and fraction available water in two soil layers, the first year's simulation in LH is designed to run twice. Soil moisture of each layer is updated at daily time-step on the basis of previous day's soil moisture through balancing the amount of water infiltrating into soil and that removed from two soil layers through runoff, percolation and actual ET.

2.2 The parameterization of LH model

The land cover-related parameters (or attributes) in LH can be classified into two categories: (i) parameters that govern dynamics of water balance in the soil-vegetation-atmosphere systems (Table 1), and (ii) parameters that are necessary for simulating plant photosynthesis (Table 2). The first category involves leaf longevity, the fraction of roots in two soil layers, the minimum water scalar value at which leaves are shed by drought-deciduous vegetation, the canopy conductance component that is not associated with photosynthesis, the maximum transpiration rate, and interception storage of vegetation.

Specifically, the leaf longevity of each vegetation type is used to calculate its leaf area. The fraction of roots in two soil layers (f_1 and f_2, dimensionless) affects relative soil mositure (wr, dimensionless) that is given by:

$$\mathrm{wr} = w_1 \times f_1 + w_2 \times f_2 \quad (1)$$

where w_1 and w_2 are the fractions of available water (dimensionless, <1.0) in the upper and lower layer of soil, respectively. The minimum water scalar (Wmin) adjusts daily drought leaf phenology because drought-deciduous plants shed their leaves when their water scalar falls below a specific threshold. The canopy conductance component (CaC) (mm s^{-1}) is a part of total non-water-stressed canopy conductance (gp) (mm s^{-1}) averaged over a grid cell as follows (Haxeltine and Prentice, 1996):

$$\mathrm{gp} = ((1.6 \times \mathrm{adt}/(\mathrm{ca} \times (1.0 - \lambda)))/Dt\mathrm{s}) + \mathrm{CaC} \quad (2)$$

HESSD
9, 1207–1249, 2012

where adt (mm) is daily gas converted from daytime net photosynthesis; *ca* is the mole fraction of atmospheric CO_2; λ is the optimal ratio of intercellular to ambient CO_2 concentration; and *Dt*s refers to the length of daylight in seconds.

The maximum daily transpiration rate (Emax) (mm) is used to simulate the water supply function (S) (mm) through the following expression:

$$S = E\max \times wr \times ph_d \times fvc \quad (3)$$

where ph_d is daily leaf phenology (dimensionless) of a vegetation type and fvc is foliar vegetative cover (%) in a grid cell. The vegetation-specific interception storage (Ints) (mm) is related to the interceptation storage parameter (Intc) (dimensionless) and calculated as follows (Kergoat, 1998):

$$Ints = \min(Pr, Intc \times LAI \times ph_d \times Pr) \quad (4)$$

where LAI ($m^2\,m^{-2}$) is leaf area index and Pr (mm) is daily precipitation.

Parameters needed for simulating plant photosynthesis the second category include the maximum foliar N content (Nmax) ($mg\,g^{-1}$), the low (T_1) and high (T_2) temperature limit for CO_2 uptake, and the lower (T_l) and upper (T_h) ranges of optimum temperature for plant photosynthesis (Table 2). These parameters are used to calculate total daytime net photosynthesis of plant and to convert daytime net photosynthesis to gas using an ideal gas equation (Haxeltine and Prentice, 1996), which is later used to simulate canopy conductance (see Eq. 2). The specific value of each parameter is based on published literatures (e.g., Smith et al., 2001; Sitch et al., 2003).

2.3 The calculation of major hydrologic variables

The calculation of each hydrologic variable in LH is almost the same as that described in Gerten et al. (2004). We briefly introduce the calculation of major output variables (see Fig. 1) for reference. Daily equilibrium PET rate (E_{eq}) (mm) is expressed as:

$$E_{eq} = \left[\frac{\Delta}{\Delta + \gamma}\right]\frac{R_n}{L} \quad (5)$$

HESSD
9, 1207–1249, 2012

where R_n ($Jm^{-2}d^{-1}$) refers to net radiation calculated from latitude, day of the year, sunshine hours and air temperature; Δ is the rate of saturation vapor pressure increase with temperature; γ ($Pa\,K^{-1}$) and L ($J\,Kg^{-1}$) are the psychrometric values of air and the latent heat of water vaporization adjusted by daily temperature, respectively. To avoid abrupt change in values of variables such as the ratio of ET to PET in high latitudes, LH assigns daily E_{eq} a value 10^{-6} when the calculated E_{eq} is zero. Since the equilibrium potential evapotranspiration (E_{eq}) rarely occurs in the real world, the Priestley-Taylor coefficient (α) with values that may vary from 1.26 (for well watered land) to 1.4 (for dry land) is used to estmate potential evapotranspiration (E_p) at different locations as follows:

$$E_p = E_{eq} \times \alpha \tag{6}$$

Actual ET is the sum of interception loss, vegetation transpiration and evaporation from soil. Daily interception loss (L)(mm) is a product of daily PET (E_p) and the fraction of day-time (ω) (dimensionless) when canopy is wet as follows:

$$L = E_p \times \omega \tag{7}$$

The value of ω is related to the canopy interception storage capacity. Vegetation transpiration is estimated based on a comparison between an atmosphere-controlled demand function and a plant-controlled supply function (see Eq. 3).

Daily evaporation (E_s) (mm) from soil follows Huang et al. (1996) as:

$$E_s = E_p wr(1 - fvc) \tag{8}$$

where wr represents the relative moisture in the upper layer of the soil column; fvc is again foliar vegetative cover (%) as in Eq. (3).

Daily soil water content in both layers at day i is updated taking account of the water content at previous day, snowmelt (M_i) (mm), throughfall (Pr_T), transpiration

HESSD
9, 1207–1249, 2012

($E_{T,i}$) (mm), evaporation ($E_{s,i}$) (mm), percolation ($p_{1,i}$) (mm) through two layers and runoff ($R_{1,i}$) (mm) during the current day i:

$$\begin{cases} \Delta w_{1,i} = \Delta w_{1,i-1} + \mathrm{Pr}_{t,i} + M_i - \beta_{1,i} \times E_{T,i} - E_{s,i} - p_{1,i} - R_{1,i} \\ \Delta w_{2,i} = \Delta w_{2,i-1} + p_{1,i} - \beta_{2,i} \times E_{T,i} - R_{2,i} - p_{2,i} \end{cases} \quad (9)$$

where $\Delta w_{1,i}$ and $\Delta w_{2,i}$ (mm) are daily changes in soil water content of both layers at day i; β_1 and β_2 represent the fractions of water extracted for transpiration from each layer ($\beta_1 + \beta_2 = 1$). The model simulates surface runoff ($R_{1,i}$) and subsurface runoff ($R_{2,i}$) from the excess of water over field capacity of the upper and lower soil layer, respectively. The total runoff in a grid cell is the sum of surface and subsurface runoff.

Unlike its predecessor LPJ-DGVM (version 1.2) that only uses temperature as an index to estimate snowmelt, LH considers effects of both solar radiation and temperature on snowmelt (mm) at day i as follows (e.g. Kane et al., 1997):

$$M_i = \begin{cases} c1 \times (1 - \mathrm{Sal}) \times \mathrm{dr_i} \times \mathrm{dl_i} & \text{if } T_{\mathrm{air}} < T_{\mathrm{snow}} \\ (c1 \times (1 - \mathrm{Sal}) \times \mathrm{dr_i} \times \mathrm{dl_i} + c2 \times (T_{\mathrm{air}} - T_{\mathrm{snow}})) \times \mathrm{Pr} & \text{if } T_{\mathrm{air}} >= T_{\mathrm{snow}} \end{cases} \quad (10)$$

where, Sal is snow albedo; dr_i (W $\mathrm{m}^{-2}\mathrm{hr}^{-1}$) is down net shortwave radiation flux in day i; dl_i (hr) is day length in day i; T_{air} (°C) is daily air temperature, T_{snow}(°C) is temperature (0 °C) at which snow occurs; Pr (mm) is daily precipitation; $c1$ and $c2$ are empirical coefficients.

2.4 Model input data

Our monthly mean temperature (°C) and precipitation (mm) at 2.5 arc-min grid cells are developed by the PRISM (Parameter-elevation Regressions on Independent Slopes Model) Climate Group (Daly et al., 2000, 2002) and available from http://www.prism.oregonstate.edu/. Monthly percent sunshine (%) and wet-day frequency (days) are derived from the CRU TS 3.0 data sets from the Climatic Research Unit (CRU) at the University of East Anglia (UK) (Mitchell and Jones, 2005). We interpolated 0.5 degree CRU wet-day frequency data onto PRISM 2.5-arc min elevation points following the

HESSD
9, 1207–1249, 2012

approach described in Tang and Beckage (2010), in which we first fitted a regression model to CRU 0.5 degree data that treats climatic value at each grid cell as a function of its latitude, longitude and elevation to estimate the local lapse rate of wet-day frequency. The calculated local lapse rate was then used to interpolate CRU data to PRISM 2.5 arc-min resolution by considering the elevation differences between CRU points and targets from PRISM 2.5 arc-min elevation data. These adjusted climatic values for PRISM points were bilinearly interpolated to obtain the value of a climate variable at a target point. The CRU sunshine data were downscaled by bilinear interpolation.

The global land cover classification from Global Land Cover Facility (GLCF) at the University of Maryland (http://glcf.umiacs.umd.edu/data/vcf/) are used to define land cover input at each grid cell that is most likely to exist in the study region. After excluding water, we grouped the rest of 13 GLCF land cover classes into 11 types (Table 1). These land cover types were regridded onto PRISM 2.5-arc min elevation points. The GLCF Vegetation Continuous Fields (VCF) data (Hansen et al., 2000, 2003) are used to define foliar vegetative cover (%) of a GLCF-based land cover in a grid cell. The VCF data contain proportional estimates for three cover types: woody vegetation, herbaceous vegetation and bare ground. The total percentage cover for these three cover types in a grid cell is 100 percent (Hansen et al., 2000).

The soil data were derived from Miller and White (1998) soil texture classes that were gridded at 250 m spatial resolution (http://www.soilinfo.psu.edu/). These soil texture classes were based on the State Soil Geographic (STATSGO) Database distributed by the United States Department of Agriculture Natural Resources Conservation Service. We reclassified 16 standard soil classes in STATSGO data into 8 classes to match those defined in both LH and LPJ-DGVM. The soil data were regridded onto 2.5 arc-min PRISM elevation points. Annual atmospheric CO_2 concentrations for the period 1951–2006 were from the Climate Research Group at the University of Illinois at Urbana-Champaign (Schlesinger and Malyshev, 2001).

HESSD
9, 1207–1249, 2012

2.5 Model testing data and approaches

Several existing sets of observed or simulated data using different methods were used to test the LH's performance in simulating ET, soil moisture and surface runoff for the coterminous US (Table 3). The German ET data for the Everglades of Florida (US) (German, 2000) was evaluated on the basis of the Bowen-ratio energy budget method (Bowen, 1926). All data needed for application of the Bowen-ratio method, including net radiation, soil temperature, water level, air temperature and vapor pressure, were measured at 15-min intervals spanning from 1996 to 2001 and at 9 sites ranging from 24.75° N to 26.25° N and from 79.75° W to 81.25° W (German, 2000). The Vörösmarty ET data (Vörösmarty et al., 1998) were computed using a global-scale water balance model that considered effects of wind speed and vapor pressure on surface hydrology.

Illinois soil moisture data consist of total soil moisture measured at 19 stations in Illinois of the US. These data span an interval from January 1981 to June 2004 and were calibrated with gravimetric observations. We did not use first three years' (1981, 1982 and 1983) data for comparison because they have smaller variability than the rest of data (Hollinger and Isard, 1994). Iowa soil moisture data consist of observations from two catchments located at 41.2° N and 95.6° W. Each catchment has three sites where soil moisture observations were made. These data provide a 23 yr record spanning from 1972 to 1994. However, observations were mostly made between April and October (Entin, 1998; Entin et al., 2000). Both Illinois and Iowa soil moisture data are available from the Global Soil Moisture Data Bank (Robock et al., 2000). When necessary, we converted measured soil moisture into millimeter to match the LH-simulated. We only used soil moisture in the top 50 cm of soil layers because other information such as soil density for the rest of layers might not be available for the unit conversion.

The Global Runoff Data Centre (GRDC) composite runoff fields (CRF) (Fekete et al., 2002) were used to evaluate the spatial pattern of LH-simulated annual runoff for the coterminous US. The GRDC CRF was developed by combining observed river discharge information with climate-driven water balance model outputs. The observed

HESSD
9, 1207–1249, 2012

discharge was derived from selected gauging stations from the World Meteorology Organization GRDC data archive. These station data were coregistered to a simulated topological network at 0.5 degree land grid.

The US Geological Survey (USGS) water data from 13 river gage stations (Table 4) were used to test LH-simulated surface runoff over the years 1981–2006. We select 13 rivers for comparison because (i) the derived watersheds from 13 gage stations cover most of the coterminous US (Supplement Fig. S1), and (ii) the observed discharge information might not always be available for other rivers over the study period. We converted simulated surface runoff (mm) into cubic meter per second ($m^3 s^{-1}$) under the assumption that modeled surface runoff at all grid cells inside a watershed flows out its gage station within a given month. The conversion of modeled surface runoff into stream flow (f_{LH}, j) in month is expressed as:

$$f_{LH,j} = (\Sigma_{i=1}^{n} srf/_{n}) \times \frac{DA}{Days_j \times 86400} / 1000 \quad (11)$$

where srf is LH-simulated surface runoff (mm) at grid cell i in month j; n is the number of grid cells inside a watershed; DA is the drainage area (m^2) for a gage station; $Days_j$ is the number of days in month j. We also converted the USGS stream flow data from cubic feet per second into cubic meter per second for comparison.

We used statistics such as adjusted R square (R^2), root mean squared errors (RMSE) and Nash-Sutcliffe coefficient (Nr) (Nash and Sutcliffe, 1970) as appropriate to quantify the agreement between modeled and simulated/observed ET, soil moisture and surface runoff. For example, the Nash-Sutcliffe coefficient is mainly used to quantify the agreement between modeled and observed stream flow for 12 major rivers (the Alabama River and the Apalachicola River are combined into the "Alabama River" for comparison) in the coterminous US and expressed as follows:

$$Nr = 1 - \frac{\Sigma_{i=1}^{n}(Q_i - Q_m)^2}{\Sigma_{i=1}^{n}(Q_i - \bar{Q})^2} \quad (12)$$

HESSD
9, 1207–1249, 2012

where, Q_i is observed stream flow in month i; Q_m is modeled stream flow in month i; $\bar{Q}$ is long-term average monthly stream flow; and n is the total number of months.

2.6 The application of LPJ-DGVM for the coterminous US

In order to test if LH performs at least as well as LPJ-DGVM (hereafter DGVM) in simulating the land surface water balance, we also ran the DGVM for the coterminous US using historical climate and CO_2 data for the period 1951–2006 (climate and CO_2 data for the period 1982–2006 are same between the two model simulations) and the same soil data. To minimize effects of parameters' uncertainty on modeled land surface water balance, we kept values of the same parameters between the two model simulations identical. Following the general protocol, we first span-up the DGVM simulation for 1000 yr using climate and CO_2 data for the period 1951–1980. The 1000 yr spin-up is viewed as the maximum number of years required for vegetation and soil pools to reach equilibrium state with long-term climate (Sitch et al., 2003). Following the spin-up simulation, the DGVM was continuously run using climate and CO_2 data for the period 1981–2006. Since we kept values of the same parameters between LH and DGVM simulations identical for comparison, the DGVM-simulated surface hydrology and vegetation distribution were not evaluated and could even be biased.

3 Results

3.1 The LH-simulated actual ET and its evaluation

LH-simulated annual actual ET averages 536 mm in the study region and varies from 0 to 1305 mm among grid cells (Fig. 2a). The lowest ET is modeled to occur in southeastern California of the US where annual precipitation is low (<160 mm) but temperature is high (>21 °C) (Supplement Fig. S2). The highest ET is modeled to occur in coastal areas of southern and southeastern US where both annual precipitation (>1400 mm) and temperature (>20 °C) are high. In the eastern US, annual ET is modeled to decrease

HESSD
9, 1207–1249, 2012

from south to north (Fig. 2a), a result of temperature-related latitudinal gradients (Supplement Fig. S2). In the western US, annual ET is modeled to be less than 600 mm in most areas and does not decrease in latitudinal direction. In some mountain ranges of the western US, such as in the Pacific Coastal Ranges, simulated annual ET ranges from 600 to 900 mm (Fig. 2a), attributing to high annual precipitation (> 2600 mm) in these areas (Supplement Fig. S2).

The magnitudes of LH-simulated annual ET among grid cells agree well with those from Vörösmarty ET data (Vörösmarty et al., 1998). For example, mean annual ET (533 mm) under LH-simulation is close to 572 mm from Vörösmarty ET. The range (0 to 1305 mm) of LH-simulated annual ET is similar to the range of 53 to 1414 mm of Vörösmarty ET data. The standard deviation of LH-simulated annual ET is 238 mm, close to 269 mm from Vörösmarty ET data. The spatial pattern of LH-simulated ET (Fig. 2a) visually agree well with that pictured by Vörösmarty ET data (Fig. 2b). For example, annual ET in both data sets decreases from more than 1200 mm in the southern and southeastern US to below 600 mm in the north in eastern US. In the western US, annual ET varies from 0 to 600 mm in most areas except for mountain ranges (Fig. 2).

LH-simulated monthly ET (average for all grid cells in a watershed) is strongly correlated ($R^2 > 0.72$, $p < 0.01$) with those from Vörösmarty ET data in 12 river watersheds (Fig. 3 and Fig. S1), indicating that LH captures well the variation of monthly ET illustrated in Vörösmarty ET data. Average monthly ET (12 month's mean) under LH simulation is close (difference <10 %) to those from Vörösmarty ET data in the Sacramento (37 mm), Snake (27 mm), Missouri (41 mm), Mississippi (55 mm), Ohio (61 mm), Connecticut (43 mm), Susquehanna (46 mm), Colorado (48 mm) and Arkansas (47 mm) River watersheds, respectively. Major differences occur in estimates of monthly ET for the Willamette, Alabama and Wateree River watersheds, in which LH-simulated monthly ET is 19 % higher, 16 % and 20 % lower than Vörösmarty monthly ET, averaging 51, 79 and 90 mm, respectively. In more detail, LH-simulated ET in late spring and early summer in most watersheds (except for the Willamette River watershed) is less than those from Vörösmarty ET data (Fig. 3).

HESSD
9, 1207–1249, 2012

When compared to local ET data in the everglades of Florida, LH-simulated monthly ET over the years 1996–2001 corresponds well ($R^2 = 0.61$, $p < 0.01$) to the measured data in these regions (German, 2000) (Fig. 4). LH-simulated monthly ET averages 91 mm, approximating 94 mm of German ET. The standard deviation of LH-simulated monthly ET is 24 mm, close to 25 mm of German ET data. In addition, LH-simulated monthly ET ranges from 47 to 144 mm, within the range of German ET varying from 29 to 153 mm. The root mean square error (RMSE) between LH-simulated and German monthly ET is 18.5, less than 21 % of average monthly ET for both compared data.

3.2 The LH-simulated soil moisture and its evaluation

LH-simulated annual soil moisture averages 107 mm in the study region and ranges from 0 to 325 mm among grid cells (Fig. 5). Annual soil moisture is modeled to be highest in mountain areas, such as in the Pacific Coastal Ranges, the Cascade Mountains of Oregon, and the Appalachian Mountains in the eastern and the northeastern US (Fig. 5). In these areas, LH-simulated annual soil moisture is beyond 160 mm, attributing to low regional annual temperature (<9 °C) and high precipitation (>1500 mm). Annual soil moisture is modeled to be low (< 100 mm) in most western US. In these regions, annual precipitation is relatively low (<400 mm) while annual mean temperature can be more than 9 °C (Fig. A.2b).

When LH-simulated monthly soil moisture (averaged for all grid cells ranging from 88.25° W to 91.25° W and from 37.25° N to 42.25° N, a spatial extent that approximately matches the extent of Illinois soil moisture) was compared to Illinois soil moisture (Hollinger and Isard, 1994), the statistics ($R^2 = 0.79$, $p < 0.01$) suggest that LH captures well the variation of monthly soil moisture in this region over the years 1984–2001 (Fig. 6a). LH-simulated monthly soil moisture averages 160 mm, equaling 160 mm from observed data. LH-simulated monthly mean value ranges from 87 to 202 mm over the period 1984–2001, resembling observed values that range from 86 to 201 mm. The standard deviation of LH-simulated soil moisture is 29.3 mm, close to 28.9 mm from the observations. The RMSE between LH-simulated and observed values for 246 months

HESSD
9, 1207–1249, 2012

is 14, indicating that LH simulates well monthly soil moisture in this region although it may under- or overestimate soil moisture in some months (Fig. 6a).

Additional comparison against observed soil moisture in two catchments of Iowa still suggests that LH is able to capture the variation of monthly soil moisture at local scale as indicated by the coefficient ($R^2 = 0.40$, $p < 0.01$) between two compared data sets (Fig. 6b). For the whole period 1982–2004, LH-simulated monthly soil moisture averages 149 mm, only 10 mm lower than from observed data (159 mm). LH-simulated monthly soil moisture ranges from 76 to 208 mm, a slightly broader range than observed values (93 to 201 mm). Nevertheless, LH-simulated soil moisture in this particular region is comparatively more variable than observed values, as indicated by the standard deviation of 26 mm for LH and 34 mm for observation. The RMSE between LH-simulated and observed values for 91 points is 29, accounting for 18 % of observed mean monthly soil moisture.

3.3 The LH-simulated surface runoff and its evaluation

LH-simulated annual surface runoff averages 234 mm in the study region and ranges from 0 to 6440 mm among grid cells with a standard deviation of 307 mm (Fig. 7a). As was the case for annual soil moisture, surface runoff is modeled to be highest in mountain areas, such as in the Pacific Coastal Ranges, the Cascade Mountains of Oregon and Washington, and the Appalachian Mountains in eastern and northeastern US. In these regions, annual precipitation is comparatively high while annul temperature is comparatively low (Supplement Fig. S2). Annual surface runoff is modeled to be low in most western US, attributing to low annual precipitation (<400 mm). Overall, LH-simulated surface runoff is above 200 mm in eastern US but below 200 mm in western US (Fig. 7a).

The magnitudes of LH-simulated surface runoff agree well with the GRDC CRF data (Fig. 7b). Annual surface runoff averages 215 mm in the GRDC CRF data, which is only 19 mm lower than LH-simulated annual surface runoff (234 mm) for the coterminous US. The spatial pattern of LH-simulated annual surface runoff is consistent with that

HESSD
9, 1207–1249, 2012

pictured by the GRDC CRF data (Fig. 7a, b). For example, both data show that annual surface runoff is above 200 mm in eastern US but below 200 mm in western US. In addition, annual surface runoff in both compared data sets is relatively high in mountain areas such as in the Pacific Coastal Ranges and the Appalachia Mountains in eastern US. Nevertheless, the upper range of LH-simulated annual surface runoff (6440 mm) is about 2.5 times the composite one (2577 mm). The standard deviation of LH-simulated surface runoff (307 mm) is larger than that of the GRDC CRF data (278 mm), indicating that LH-simulated annual surface runoff is more variable in the study region relative to the GRDC CRF.

Further comparison of LH-simulated monthly stream flow (converted from modeled surface runoff) to the USGS water data demonstrates that LH is able to correctly simulate the variations of monthly stream flow in most 12 major rivers in the coterminous US, as indicated by the statistics ($R^2 > 0.50$, $p < 0.01$; Nr > 0.51 (Moriasi et al., 2007)) calculated for the 12 rivers (Fig. 8). Especially for watersheds where forest is dominant land cover (Supplement Fig. S3), LH-simulated monthly stream flow agree well ($R^2 > 0.65$, $p < 0.01$; Nr > 0.52) with observed values over the years 1982–2006. These rivers involve the Willamette (R^2=0.85; Nr = 0.74), Ohio (R^2 = 0.71; Nr = 0.65), Susquehanna (R^2=0.69; Nr = 0.68), Connecticut (R^2 = 0.67; Nr = 0.56) and Wateree (R^2 = 0.69; Nr = 0.51) (Fig. 8). In contrast, for watersheds where grass, shrubs and/or crops are dominant land covers, the agreement between compared data is weaker ($R^2 < 0.65$). These rivers involve the Snake (R^2 = 0.64; Nr = 0.52), Missouri (R^2=0.50; Nr = 0.30), Mississippi (R^2 = 0.56; Nr = 0.52) and Colorado (R^2=0.53; Nr = 0.22), excepting the Arkansas River for which the modeled monthly stream flow agrees well (R^2 = 0.59; Nr = 0.58) with the observed.

The magnitudes of LH-simulated mean monthly stream flow over the years 1982–2006 are close (difference <11 %) to measured mean monthly stream flow for most 12 rivers, including the Willamette, Snake, Missouri, Mississippi, Ohio, Connecticut, Susquehanna, Wateree, and Alabama River (Table 5). Major difference occurs in estimates of monthly mean stream flow for the Sacramento and Colorado. For these two

HESSD
9, 1207–1249, 2012

rivers, LH-simulated average monthly stream flow is 24.0 % higher and 19.6 % lower than their counterparts from measured data, averaging 346.6 and 79.9 $m^3 s^{-1}$, respectively (Table 5). Although LH-simulated mean monthly flow is similar to that derived from observed values in most rivers, it is more variable than measured monthly stream flow for most rivers over the years 1982–2006 as indicated by the magnitudes of standard deviations for each of compared data sets (Table 5).

3.4 Comparison between LH- and DGVM-simulated hydrological data

LH-simulated monthly ET correlates well ($R^2 > 0.71$, $p < 0.01$) with DGVM-simulated in 12 river watersheds (Fig. 9a–i). The correlation is weakest in the Connecticut and Susquehanna River watersheds but the calculated adjusted R square statistic is still as high as 0.71 and 0.72, respectively. Major differences occur in estimates of monthly ET in spring and early summer in the Sacramento, Ohio, Connecticut, Susquehanna and Wateree River watersheds, in which LH-simulated average monthly ET is about 14 %, 17 %, 30 %, 26 % and 14 % lower than DGVM-simulated, averaging 44.3 mm in the Sacramento river watershed, 71.3 mm in the Ohio River watershed, 57.7 in the Connecticut River watershed, 62.1 mm in the Susquehanna River watershed and 77.0 mm in the Wateree River watershed. In other watersheds, difference between LH- and DGVM-simulated average monthly ET is less than 12 %.

LH-simulated soil moisture in the top 50 cm of soil layers strongly correlates ($R^2 > 0.71$, $p < 0.01$) with DGVM-simulated in most watersheds (Fig. 9m-x) except for the Colorado ($R^2 = 0.62$, $p < 0.01$) (Fig. 9u) and Arkansas River watersheds ($R^2 = 0.37$, $p < 0.01$) (Fig. 9x). However, the magnitude of LH-simulated average monthly soil moisture is distinct from DGVM-simulated in the Sacramento, Snake, Missouri, Connecticut, Susquehanna, Colorado and Arkansas River watersheds. The difference is larger in watersheds where grass, shrubs and/or crops are dominant land covers than in watersheds where forests are dominant. For example, LH-simulated monthly soil moisture is about 33 %, 34 %, 32 % and 46 % higher than DGVM-simulated in the Snake (58 mm), Missouri (64 mm), Colorado (52 mm) and Arkansas River (59 mm)

HESSD
9, 1207–1249, 2012

watershed, respectively. In contrast, it is about 15 % and 17 % higher than DGVM-simulated in the Connecticut (158 mm) and Susquehanna River (153 mm) watershed, respectively. In other watersheds, difference between compared monthly ET is less than 10 %.

LH-simulated average monthly stream flow is linearly correlated ($R^2 > 0.61$, $p < 0.01$) with DGVM-simulated in watersheds where forests dominate, including the Sacramento ($R^2 = 1.00$), Willamette ($R^2 = 0.98$), Ohio ($R^2 = 0.96$), Connecticut ($R^2 = 0.71$), Susquehanna ($R^2 = 0.61$), Wateree ($R^2 = 0.94$) and Alabama ($R^2 = 0.98$) Rivers (Fig. 9y, x, sf, sr, sg, sh, si). For watersheds where grass, shrub and/or crops are dominant land covers, the strength of correlation is relatively weaker. Especially for the Missouri (Fig. 9ab) and Mississippi Rivers (Fig. 9ac), the adjusted R square statistic is as low as 0.10 and 0.46, respectively. In addition, LH-simulated average monthly stream flow is much larger than DGVM-simulated in most rivers, ranging from 7.4 % higher for the Willamette River to 58.8 % higher for the Susquehanna River. However, it is about 26.3 % lower than DGVM-simulated in the Colorado River (102 $m^3 s^{-1}$).

4 Discussion

We used a list of existing data sets, both observed and simulated using different methods, to test the LH's performance in the coterminous US. These data may represent a smaller area (e.g., Illinois and Iowa soil moisture) compared to the study region. Also, the spatial resolution of testing data (e.g., 0.5-degree Vörösmarty ET and the GRDC CRF) may not match LH-simulated at 2.5 arc-min grid cells. These discrepancies might affect model's overall assessment (Liang et al., 2004). We believe, however, they do offer the possibility to test LH's performance in the study region, as illustrated by those comparisons using observed data. In addition, our simulation uses finer climate data and is likely to capture better the spatial variations of three hydrological variables than previously published data at coarser resolution as illustrated in other studies (e.g., Liu and Yang, 2010). For example, LH-simulated surface runoff (>2577 mm) is higher than

HESSD
9, 1207–1249, 2012

the GRDC CRF (<2577 mm) in the Pacific Coastal Ranges and the Cascades Mountains of Oregon where annual precipitation can vary from 3000 to 6800 mm (Daily et al., 2000, 2002). The strong correlation (R^2=0.85, Fig. 8b) and the almost equivalence (Table 5) between LH-simulated and measured monthly stream flow for the Willamette River justifies LH's ability in this region.

We note, however, much effort is still needed to improve LH's accuracy in simulating the land surface water balance at local to regional scales. LH at its current stage of development considers only radiative effects (temperature and solar radiation) while ignores aerodynamic effects on the land surface water balance. In fact, the aerodynamic factors such as vapor pressure and humidity play important roles in determining actual ET (Stoughton et al., 2002; Brunel et al., 2006; Rim, 2008) and thus the land surface water balance. Actual ET is considered to increase as vapor pressure deficit increases, which helps explain why LH-simulated monthly ET in summer is less than Vörösmarty ET data in the Snake, Missouri, Mississippi and Arkansas River watersheds (Fig. 3c, d, e, i), largely because the latter considered effects of relative humidity and vapor pressure deficit on the land surface hydrology (Vörösmarty et al., 1998). Such difference requires that the aerodynamic factors be considered in future development of LH model.

Vegetation and crops are far from static and have important effects on the land surface water balance (Arora, 2002). Different vegetation and crops have differing physiological traits such as leaf area index and stomatal conductance, affecting plant transpiration and soil evaporation due to changes in surface albedo. Although LH incorporates static land covers, rather than dynamically simulating them, it is able to simulate the land surface water balance as well as its predecessor (Gerten et al., 2004). The good agreement between LH- and DGVM-simulated (Fig. 9) and between LH-simulated and observed (e.g., Fig. 8) monthly values of three hydrological variables in most rivers or watersheds justifies the feasibility of incorporating static land covers into DGVM to simulate the land surface water balance at large spatial scales.

HESSD
9, 1207–1249, 2012

Discrepancies between LH and DGVM simulation emerge in estimating the magnitudes of three hydrological variables. For example, LH-simulated monthly stream flow is closer than DGVM-simulated to observed values in the Willamette, Mississippi, Ohio, Connecticut, Susquehanna, Colorado, Wateree, Alabama and Arkansas River, as indicated by the absolute magnitudes of differences between modeled and observed data (Table 6). The reason is because DGVM-simulated monthly stream flow for these Rivers is much lower in spring and early summer than both LH-simulated and observed values (Fig. 9y–aj). Such difference is reversed in summer in some watersheds located at relatively high latitudes such as the Snake River watershed (Fig. 9aa). The root causes is LH considers effects of both temperature and solar radiation on snowmelt while the DGVM considers only effects of temperature on snowmelt. In addition, the DGVM-simulated potential vegetation might not match well with the predefined land covers in these watersheds (Supplement Fig. S3), which can affect modeled water balance due to differences in plant transpiration and leaf phenology. Gerten et al. (2004) found that LPJ-DGVM (version 1.2) tended to underestimate surface runoff in winter at high latitudes of the Northern Hemisphere.

Given the heterogeneity of land surface conditions and the complexity of factors affecting the land surface water balance, further improvements in model input data (e.g., soil and land covers) and model's structure are needed for LH. For example, the Sacramento River watershed has been intensely developed for water supply and the generation of hydroelectric power, which caused LH-modeled magnitudes of monthly stream flow not to agree well with the USGS observed (Fig. 8a). The vertical soil profile in LH includes only two layers, which are not enough to capture detailed physical dynamics of soil moisture (e.g., hydraulic conductivity) in soil vertical profile. The accuracy of land cover representation affects subsequent soil evaporation and plant transpiration. For example, LH-simulated ET in April, 1998 in the Everglades of Florida decreased sharply relative to March and is much lower than the measured value (Fig. 4). Land covers in the Everglades of Florida are mostly wetlands that never dry or dry only in parts of years (German, 2000). In contrast, LH (actually the GCLF data) defines land

HESSD
9, 1207–1249, 2012

cover in this area as grassland. As a result, even precipitation in April is very low (average 14 mm) while soil evaporation can be still high, resulting in higher ET measurement. The topographic factors such as slope (e.g., Quinn et al., 1998) and the intensity and frequency of rainfall events affect the convergence of surface runoff, which can cause LH-simulated stream flow not to agree well with observed discharge from gage stations. Especially in semi-arid and arid environment in western US, precipitation is thought of being important for controlling snow dominated river hydrography.

Despite the fact that much work is still needed to improve LH's accuracy, there are great advantages in modifying the DGVM for simulating large spatial scale land surface water balance. First, LH predefines land covers instead of simulating them. This greatly simplifies model's structure (Fig. 1) but does not harm model's ability in simulating land surface water balance, as was the case with its predecessor; Second, LH ignores some vegetation-related biogeographical and biogeochemical dynamics such as carbon allocation and vegetation-related parameters (Tables 1, 2) are reduced by more than half compared to its predecessor. The reduction of parameters makes LH easier grasp and parameterize in practice. This in turn enhances LH's access to users who are non-ecologists but of strong interest in large spatial land surface hydrology. Third, because LH avoids the spin-up simulations required by DGVM, plus its simplified structure, it greatly increases the computing efficiency for simulating land surface hydrology.

In addition, changes in atmospheric CO_2 concentration might affect, although arguable, the land surface water balance through inducing reduction in plants stomatal conductance and increase in plants water use efficiency (Leipprand and Gerten, 2006; Robock and Li, 2006; Felzer et al., 2009). LH couples plant photosynthesis and is able to simulate the roles of changes in CO_2 concentration in the land surface water balance. For example, our experimental simulation shows that LH-simulated annual ET under high CO_2 concentration (657 ppm) is about 30 to 75 mm lower than under low CO_2 (360 ppm) concentration in watersheds where forest is dominant land cover. The reason is that higher CO_2 concentration induces plant stomatal closure and thus

HESSD
9, 1207–1249, 2012

decreases actual ET (Heijmans et al., 2001) by reducing (about 33–73 mm) plant transpiration (e.g., Lockwood, 1999). Such effects on actual ET eventually cause soil moisture index (a ratio of actual to potential ET) to decrease by 5 % to 17 %. Vegetation will then suffer from soil moisture stress under high CO_2 concentration. The coupling of plant photosynthesis in LH is crucial for studying effects of land cover change on the land surface water balance (Kergoat et al., 2002).

5 Conclusions

According to the principle of parsimony and as Paola (2011) stated, simplification of quantitative modeling is essential if the goal is insight. LH is developed by predefining land covers, instead of simulating them as its predecessor did, for the purpose of simulating the land surface water balance at a large spatial scale. This study proves that LH is able to accurately simulate ET, soil moisture and surface runoff for the coterminous US. LH's structure is simple and straightforward. The running of LH for the land surface hydrologic study is less time-consuming and more efficient than running its predecessor. The specification of static land covers in LH does not harm model's ability to simulate the land surface water balance. The consideration of effects of solar radiation on snowmelt improves model's estimates of monthly stream flow in winter and spring. LH couples plant photosynthesis and considers the potential roles of changes in atmospheric CO_2 concentration in the land surface water balance through shifting plant's water use efficiency. These advantages justify that the modification of the DGVM for large spatial water balance simulation is valuable because such simplification can render complex problems tractable and the simplified model for hydrologic study is easier to grasp, more clearly able to connect cause and effect than its predecessor, especially in the context of effects of climate and land cover change on the land surface water balance.

HESSD
9, 1207–1249, 2012

Supplementary material related to this article is available online at: http://www.hydrol-earth-syst-sci-discuss.net/9/1207/2012/hessd-9-1207-2012-supplement.pdf.

Acknowledgements. Research was supported by NSF grant numbers ATM 0602409 and the Department of Geography at the University of Oregon. We greatly appreciate all developers of the Lund-Potsdam-Jena (LPJ) dynamic global vegetation model, with special thanks to Dieter Gerten for developing the surface-hydrology model embedded in LPJ-DGVM. We thank Andrew Marcus and Sarah Shafer for their comments on Tang's PhD thesis. We appreciate Sony Pradhanang for her discussion of the USGS stream flow data.

References

Arora, V.: The use of the aridity index to assess climate change effect on annual runoff, J. Hydrol., 265, 164–177, 2002.

Arora, V. and Boer, G.: The temporal variability of soil moisture and surface hydrological quantities in a climate model, J. Climate., 19, 5875–5888, 2006.

Bowen, I. S.: The ratio of heat losses by conduction and by evapotranspiration from any water surface, Phys. Rev., 27, 779–787, 1926.

Brabson, B. B., Lister, D. H., Jones, P. D., and Palutikof, J. P.: Soil moisture and predicted spells of extreme temperatures in Britain, J. Geophys. Res., 110, D05104, doi:10.1029/2004JD005156, 2005.

Brunel, J. P., Ihab, J., Droubi, A. M., and Samaan, S.: Energy budget and actual evapotranspiration of an arid oasis ecosystem: Palmyra (Syria), Agr. Water Manage., 84, 213-220, 2006.

Daly, C., Gibson, W. P., Taylor, G. H., Johnson, G. L., and Pasteris, P.: A knowledge-based approach to the statistical mapping of climate, Clim. Res., 22, 99-113, 2002.

Daly, C., Taylor, G. H., Gibson, W. P., Parzybok, T. W., Johnson, G. L., and Pasteris, P.: High-quality spatial climate data sets for the United States and beyond, T. Am. Soc. Agri. Eng., 43, 1957–1962, 2000.

Engstrom, R., Hope, A., Kwon, H., Harazono, Y., Mano, M., and Oechel, W.: Modeling

HESSD

9, 1207–1249, 2012

evapotranspiration in Arctic coastal plain ecosystems using a modified BIOME-BGC model, J. Geophys. Res-Biogeo., 111, G02021, doi:10.1029/2005JG000102, 2006.
Entin, J. K.: Spatial and temporal scales of soil moisture variations. Ph.D. dissertation, Department of Meteorology, University of Maryland, 125 pp. 1998.
Entin, J. K., Robock, A., Vinnikov, K. Y., Hollinger, S. E., Liu, S., and Namkhai, A.: Temporal and spatial scales of observed soil moisture variations in the extratropics, J. Geophys. Res., 105, 11865–11877, 2000.
Evans, S. and Trevisan, M.: A soil water-balance bucket model for paleoclimatic purposes. 1. model structure and validation, Ecol. Model., 82, 109–129, 1995.
Fekete, B. M., Vörösmarty, C. J., and Grabs, W.: High-resolution fields of global runoff fields of observed river discharge and simulated water balances, Global Biogeochem. Cy., 16, 1042, doi:10.1029/1999gb001254, 2002.
Felzer, B. S., Cronin, T. W., Melillo, J. M., Kicklighter, D. W., and Schlosser, C. A.: Importance of carbon-nitrogen interactions and ozone on ecosystem hydrology udring the 21st century, J. Geophys. Res.-Biogeo., 114, G01020, doi:10.1029/2008JG000826, 2009.
German, E. R.: Regional evaluation of evapotranspiration in the Everglades: US Geological Survey Investigations Report 00-4217, 48 pp., 2000
Gerten, D., Schaphoff, S., Haberlandt, U., Lucht, W., and Sitch, S.: Terrestrial vegetation and water balance – hydrological evaluation of a dynamic global vegetation model, J. Hydrol., 286, 249–270, 2004.
Glenn, E. P., Huete, A. R., Nagler, P. L., Hirschboeck, K. K., and Brown, P.: Integrating remote sensing and ground methods to estimate evapotranspiration, CRC Cr. Rev. Plant Sci., 26, 139–168, 2007.
Hansen, M., DeFries, R. S., Townshend, J. R. G., Carroll, M., Dimiceli, C., and Sohlberg, R. A.: Global percent tree cover at a spatial resolution of 500 m: first results of the MODIS vegetation continuous fields algorithm, Earth Interac., 7, 1–15, 2003.
Hansen, M. C., DeFries, R. S., Townshend, J. R. G., and Sohlberg, R.: Global land cover classification at 1km spatial resolution using a classification tree approach, Int. J. Remote Sens., 21, 1331–1364, 2000.
Haxeltine, A. and Prentice, I. C.: BIOME3: An equilibrium biosphere model based on eco-physiological constraints, resource availability and competition among plant functional types, Global Biogeochem. Cy., 10, 693–709, 1996.
Heijmans, M. M. P. D., Arp, W. J., and Berendse, F.: Effects of elevated CO_2 and vascular plants

HESSD
9, 1207–1249, 2012

on evapotranspiration in bog vegetation, Glob. Change Biol., 7, 817-827, 2001.
Hickler, T., Smith, B., Sykes, M. T., Davis, M. B., Sugita, S., and Walker, K.: Using a generalized vegetation model to simulate vegetation dynamics in northeastern USA, Ecology, 85, 519–530, 2004.
Hollinger, S. E. and Isard, S. A.: A soil moisture climatology of Illinois, J. Climate, 7, 822–833, 1994.
Huang, J., Van Den Dool, H. M., and Georgakakos, K. P.: Analysis of model-calculated soil moisture over the United States, 1931–1993, and applications to long-range temperature forecasts, J. Climate., 9, 1350–1362, 1996.
Kane, D. L., ASCE, M., Gieck, R. E., and Hinzman, L. D.: Snowmelt modeling at small Alaskan arctic watershed, J. Hydrol. Eng., 2, 204–210, 1997.
Kergoat, L.: A model for hydrological equilibrium of leaf area index on a global scale, J. Hydrol., 213, 268–286, 1998.
Kergoat, L., Lafont, S., Douville, H., Berthelot, B., Dedieu, G., Planton, S., and Royer., J. F.: Impact of doubled CO_2 on global-scale leaf area index and evapotranspiration: Conflicting stomatal conductance and LAI responses, J. Geophys. Res-Atmos., 107, 4808, doi:10.1029/2001JD001245, 2002.
Kosugi, Y. and Katsuyama, M.: Evapotranspiration over a Japanese cypress forest. II. Comparison of the eddy covariance and water budget methods, J. Hydrol., 334, 305-311, 2007.
Leipprand, A. and Gerten, D.: Global effects of doubled atmospheric CO_2 content on evapotranspiration, soil moisture and runoff under potential natural vegetation, Hydrolog. Sci. J., 51, 171–185, 2006.
Liang, X., Guo, J., and Leung, L. R.: Assessment of the effects of spatial resolution on daily water flux simulations, J. Hydrol., 298, 287–310, 2004.
Lockwood, J. G.: Is potential evapotranspiration and its relationship with actual evaportranspiration sensitive to elevated atmospheric CO_2 levels?, Climatic Change 41, 193–212, 1999.
Liu, J. and Yang, H.: Spatially explicit assessment of global consumptive water uses in cropland: Green and blue water, J. Hydrol., 384, 187–197, 2010.
Lu, J., Sun, G., McNulty, S. G., and Amatya, D. M.: Modeling actual evapotranspiration from forested watersheds across the Southeastern United States, J. Am. Water Resour. As., 39, 887–896, 2003.
Manabe, S., and Delworth, T.: The temporal variability of soil wetness and its impact on climate, Climatic Change 16, 185–192, 1990.

HESSD
9, 1207–1249, 2012

Miller, D. A., and White, R.A.: A conterminous United States multilayer soil characteristics dataset for regional climate and hydrology modeling, Earth Interact., 2, 1–26. 1998.
Mitchell, T. D. and Jones, P. D.: An improved method of constructing a database of monthly climate observations and associated high-resolution grids, Int. J. Climatol., 25, 693–712, 2005.
Moriasi, D. N., Arnold, J. G., Van Liew, M. W., Bingner, R. L., Harmel, R. D., and Veith, T. L.: Model Evaluation Guidelines for Systematic Quantification of Accuracy in Watershed Simulations, T. ASABE, 50, 885–900, 2007.
Murphy, S. and Lodge, G.: Surface soil water dynamics in pastures in northern New South Wales. 1. Use of electrical resistance sensors, Aust. J. Exp. Agr., 44, 273–281, 2004.
Nash, J. E. and Sutcliffe J. V.: River flow forecasting through conceptual models part I – A discussion of principles, J. Hydrol., 10, 282–290, 1970.
Paola, C.: Simplicity versus complexity, Nature, 469, 38–39, 2011.
Quinn, P. F., Ostendorf, B., Beven, K., and Tenhunen, J.: Spatial and temporal predictions of soil moisture patterns and evaporative losses using TOPMODEL and the GASFLUX model for an Alaskan catchment, Hydrol. Earth Syst. Sci., 2, 51–64, doi:10.5194/hess-2-51-1998, 1998.
Rim, C. S.: Estimating evapotranspiration from small watersheds using a water and energy balance approach. Hydrol. Process., 22, 703–714, 2008.
Robock, A. and Li, H.: Solar dimming and CO_2 effects on soil moisture trends, Geophys. Res. Lett., 33, L20708, doi:10.1029/2006GL027585, 2006.
Robock, A., Vinnikov, K. Y., Srinivasan, G., Entin, J. K., Hollinger, S. E., Speranskaya, N. A., Liu, S., and Namkhai, A.: The Global Soil Moisture Data Bank, B. Am. Meteorol. Soc., 81, 1281–1299, 2000.
Schlesinger, M. E., and Malyshev, S.: Changes in near-surface temperature and sea level for the Post-SRES CO_2-stabilization scenarios, Integrat. Ass., 2, 95–110, 2001.
Shukla, J., and Mintz, Y.: Influence of land-surface evapotranspiration on earth's climate, Science 215, 1498–1501, 1982.
Sitch, S., Smith, B., Prentice, I. C., Arneth, A., Bondeau, A., Cramer, W., Kaplan, J. O., Levis, S., Lucht, W., Sykes, M. T., Thonicke, K., and Venevsky, S.: Evaluation of ecosystem dynamics, plant geography and terrestrial carbon cycling in the LPJ Dynamic Global Vegetation Model, Glob. Change Biol. 9, 161–185, 2003.
Smith, B., Prentice, I. C., and Sykes, M. T.: Representation of vegetation dynamics in the

HESSD
9, 1207–1249, 2012

modeling of terrestrial ecosystems: comparing two contrasting approaches within European climate space. Global Ecol. Biogeogr., 10, 621–637, 2001.

Song, J., Wesely, M. L., LeMone, M. A., and Grossman, R. L.: Estimating Watershed Evapotranspiration with PASS. Part II: Moisture Budgets during Drydown Periods, J. Hydrometeorol., 1, 462–473, 2000.

Stoughton, T. E., Miller, D. R., Huddleston, E. W., and Ross, J. B.: Evapotranspiration and turbulent transport in an irrigated desert orchard, J. Geophys. Res-Atmos., 107(D20), 4425, doi:10.1029/2001JD001198, 2002.

Tang, G. and Beckage, B.: Projecting the distribution of forests in New England in response to climate change, Divers. Distrib., 16, 144–158, 2010.

Vörösmarty, C. J., Federer, C. A., and Schloss, A. L.: Potential evaporation functions compared on US watersheds: Possible implications for global-scale water balance and terrestrial ecosystem modeling, J. Hydrol., 207, 147–169, 1998.

HESSD

9, 1207–1249, 2012

Table 1. Hydrological relevant parameters for predefined land covers.

Predefined land cover types	*LeL* (yr)	*f*	*W* min	*CaC* (mm s^{-1})	*E* max (mm day^{-1})	Intc
Evergreen needleleaf forest	4.0	0.70	0.0	0.3	5.5	0.04
Evergreen broadleaf forest	2.5	0.80	0.0	0.5	5.5	0.02
Deciduous needleleaf forest	0.5	0.70	0.0	0.3	4.0	0.04
Deciduous broadleaf forest	0.5	0.70	0.0	0.5	4.0	0.02
Mixed forest	0.5	0.70	0.0	0.4	6.0	0.03
Woodland	0.5	0.80	0.0	0.3	4.0	0.02
Shrub land	0.5	0.83	0.1	0.4	5.5	0.02
Grassland	0.5	0.80	0.2	0.5	6.0	0.01
Cropland	0.5	0.80	0.2	0.5	4.5	0.01
Bare	0.5	0.75	0.0	0.0	1.0	0.00
Urban	0.5	0.75	0.0	0.0	0.0	0.00

LeL-leaf longevity; *f*-fraction of roots in soil upper layer; *W* min minimum water scalar at which leaves shed by drought deciduous biome; *CaC*-canopy conductance component that is not associated with photosynthesis; *E* max-maximum transpiration rate; *Intc*–interception storage parameter. The specific value of each parameter refers to published literatures (e.g., Sitch et al., 2003).

HESSD
9, 1207–1249, 2012

Table 2. Photosynthetic relevant parameters for predefined land covers.

Predefined land cover types	Nmax ($mg\,g^{-1}$)	T_l (°C)	T_1 (°C)	T_2 (°C)	T_h (°C)	LAI (m^2m^{-2})
Evergreen needleleaf forest	100.0	−4.0	20.0	30.0	42.0	5.1
Evergreen broadleaf forest	100.0	2.0	25.0	30.0	55.0	5.4
Deciduous needleleaf forest	100.0	−4.0	20.0	30.0	38.0	4.6
Deciduous broadleaf forest	120.0	−4.0	20.0	30.0	38.0	4.5
Mixed forest	100.0	−4.0	20.0	30.0	38.0	4.8
Woodland	100.0	−4.0	20.0	30.0	38.0	3.0
Shrub land	100.0	−4.0	15.0	30.0	45.0	2.1
Grassland	100.0	−4.0	15.0	30.0	45.0	2.5
Cropland	100.0	−4.0	15.0	30.0	45.0	4.2
Bare	0.0	−4.0	10.0	30.0	45.0	1.3
Urban	0.0	−4.0	10.0	30.0	45.0	0.3

N max is the maximum foliar N content; T_l and T_h are the low and high temperature limits for CO_2 uptake; T_1 and T_2 are the lower and upper ranges of optimum temperature for photosynthesis; LAI is short for leaf area index. The specific value of each parameter except for LAI refers to published literatures (e.g., Sitch et al., 2003). The LAI for each predefined land cover type refers to the Global Leaf Area Index Data from Field Measurements compiled at the Oak Ridge National Laboratory Distributed Active Archive Centre (DAAC) (http://daac.ornl.gov/VEGETATION/lai_des.html).

HESSD
9, 1207–1249, 2012

Table 3. Lists of observed and simulated data to test the LH's performance.

Testing data list	Methods	Temporal resolution	Size	Data sources*
(1) German ET	Composite	Monthly for 1996–2000	Plots	German (2000)
(2) Vörösmarty ET	Simulated	Monthly	0.5°	Vörösmarty et al. (1998)
(3) Illinois soil moisture	Observed	Monthly for 1981–2004	Plots	Hollinger and Isard (1994)
(4) Iowa soil moisture	Observed	Monthly for 1981–1994	plots	Entin (1998), Entin et al. (2000)
(5) The GRDC CRF	Composite	Annual	0.5°	Fekete et al. (2002)
(6) The USGS water data	Observed	Monthly for 1981–2006	Plots	http://waterdata.usgs.gov/

*Soil moisture data are available from http://climate.envsci.rutgers.edu/soil_moisture/ owned by Robock et al. (2000). The global runoff data are available from http://www.grdc.sr.unh.edu/html/Data/index.html.

HESSD
9, 1207–1249, 2012

Table 4. Details of the US Geological Survey gage stations used for model comparison.

Site name	Site number	Longitude	Latitude	Drainage area (mi^2)
1. Sacramento River at Colusa, CA	11389500	121°59′57″	39°12′51″	12 090.0
2. Willamette River at Portland, OR	14211720	122°40′00″	45°31′04″	11 200.0
3. Snake River near Anatone, WA	13334300	116°58′36″	46°05′50″	92 960.0
4. Missouri River at Hermann, MO	06934500	91°26′19″	38°42′36″	522 500.0
5. Mississippi River at Chester, IL	07020500	89°50′08″	37°54′14″	708 600.0
6. Ohio River at Metropolis, IL	03611500	88°47′27″	37°08′51″	203 000.0
7. Connecticut River at Thompsonville,CT	01184000	72°36′21″	41°59′14″	9660.0
8. Susquehanna River at Marietta,PA	01576000	76°31′52″	40°03′16″	25 990.0
9. Coolrado River at Columbus, TX	08161000	96°32′12″	29°42′22″	41 640.0
10. Wateree River near Camden, SC	02148000	80°39′15″	34°14′40″	5070.0
11. Alabama River at Claiborne,AL*	02428400	87°33′02″	31°36′54″	21 473.0
12. Apalachicola River near Sumatra,FL*	02359170	85°00′56″	28°56′57″	19 200.0
13. Arkansas River near Haskell, OK	07165570	95°38′16″	35°49′22″	75 473.0

* The Alabama and the Apalachicola River watersheds are combined together to refer to as the Alabama River watershed.

HESSD
9, 1207–1249, 2012

Table 5. Comparison between LH-simulated and observed stream flow for 12 rivers.

	The USGS stream flow (m^3s^{-1})				LH-simulated stream flow (m^3s^{-1})				Diff (%)
Rivers	min	max	mean	Std	min	max	mean	Std	
1. Sacramento	109.3	1288.4	346.6	237.9	2.1	3964.6	429.6	644.0	24.0
2. Willamette	195.4	4406.1	950.7	782.1	9.0	4872.7	951.0	972.9	0
3. Snake	276.5	3800.1	966.4	687.6	64.4	3796.7	985.5	781.9	2.0
4. Missouri	615.6	10655.6	2612.3	1577.2	347.8	17298.3	2854.2	1767.3	9.3
5. Mississippi*	709.1	13107.9	3732.4	2233.0	504.3	12184.6	3341.6	1950.7	−10.5
6. Ohio	1225.8	29421.2	8369.2	5522.2	1227.3	33323.5	7561.8	5560.2	−9.6
7. Connecticut	88.4	2098.8	516.2	357.6	93.9	2658.4	532.5	415.4	3.2
8. Susquehanna	100.0	6657.3	1096.2	868.6	204.3	5068.9	1052.2	763.1	−4.0
9. Colorado	7.2	957.1	79.9	109.1	1.8	1292.7	64.2	139.4	−19.6
10. Wateree	29.9	559.0	156.1	112.7	1.8	667.6	144.3	138.9	−7.5
11. Alabama	325.4	6232.0	1520.1	1116.5	51.0	7369.6	1421.6	1509.8	−6.5
12. Arkansas	6.2	2422.5	305.3	336.1	19.6	1763.9	276.8	249.9	−9.3

* The observed monthly stream flow subtracted that from the Missouri River in model comparison.

HESSD
9, 1207–1249, 2012

Table 6. Comparison between LH- and DGVM-simulated average monthly stream flow with reference to the observed for 12 rivers.

	Average monthly stream flow (m^3s^{-1})			Correlation (R^2)		Difference (%)	
Rivers	USGS	LH	DGVM	LH	DGVM	LH	DGVM
1. Sacramento	346.6	429.6	359.2	0.59	0.58	24.0	3.6
2. Willamette	950.7	951.0	883.1	0.85	0.85	0	−7.1
3. Snake	966.4	985.5	808.4	0.64	0.76	2.0	−16.3
4. Missouri	2612.3	2854.2	1944.7	0.50	0.64	9.3	−23.6
5. Mississippi	3732.4	3341.6	2201.5	0.56	0.50	−10.5	−41.0
6. Ohio	8369.2	7561.8	5340.4	0.71	0.64	−9.6	−36.2
7. Connecticut	516.2	532.5	371.7	0.67	0.71	3.2	−28.0
8. Susquehanna	1096.2	1052.2	664.2	0.69	0.44	−4.0	−39.4
9. Colorado	79.9	64.2	101.5	0.53	0.59	−19.6	27.1
10. Wateree	156.1	144.3	99.1	0.69	0.67	−7.5	−36.5
11. Alabama	1520.1	1421.6	1084.9	0.66	0.66	−6.5	−28.6
12. Arkansas	305.3	276.8	192.2	0.59	0.66	−9.3	−37.1

HESSD
9, 1207–1249, 2012

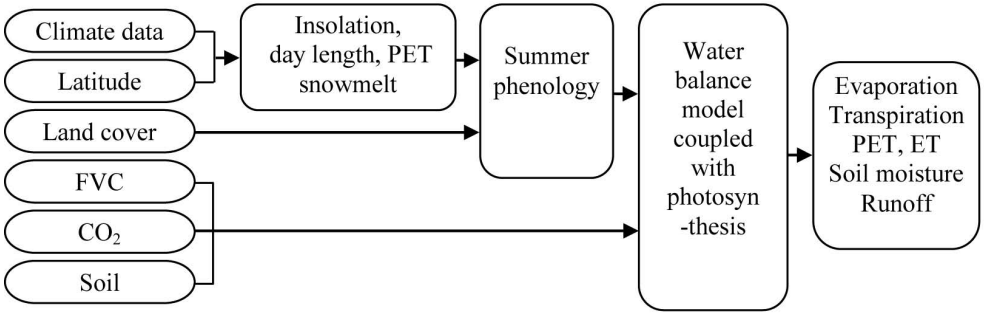

Fig. 1. A flowchart that describes the LH (LPJ-hydrology) model for calculating several hydrological variables using climate, land cover, foliar vegetative cover (FVC), CO_2 and soil data. PET and ET are short for potential and actual evapotranspiration, respectively.

HESSD
9, 1207–1249, 2012

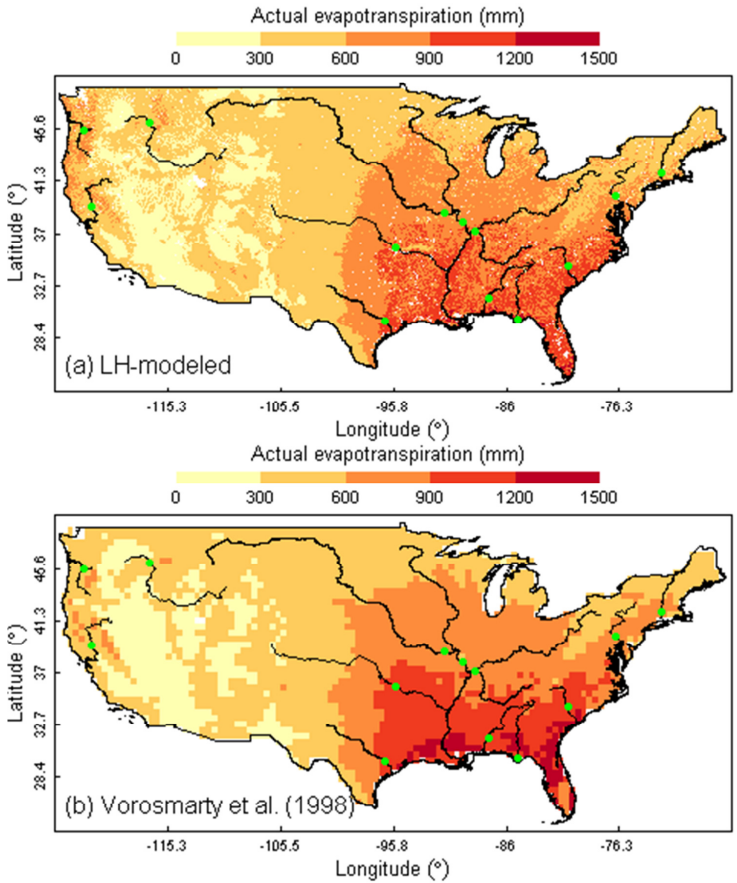

Fig. 2. (a) The LH-simulated 26-yr' (1981–2006) average annual actual ET at 2.5 arc-min grid cells; **(b)** Annual actual ET from Vörösmarty et al. (1998) at 0.5 degree grid cells. The white areas in **(a)** and **(b)** are water excluded for simulation.

HESSD
9, 1207–1249, 2012

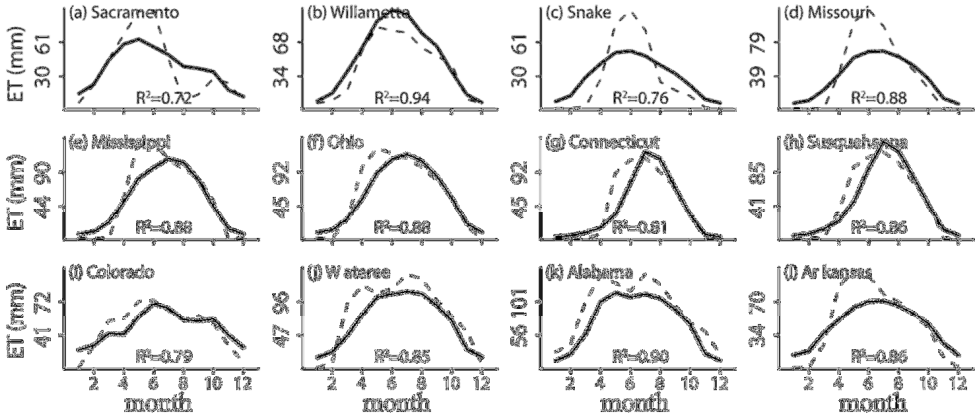

Fig. 3. Comparison between LH-simulated (solid line) and monthly ET from Vörösmarty et al. (1998) (dashed line) in the 12 river watersheds.

HESSD
9, 1207–1249, 2012

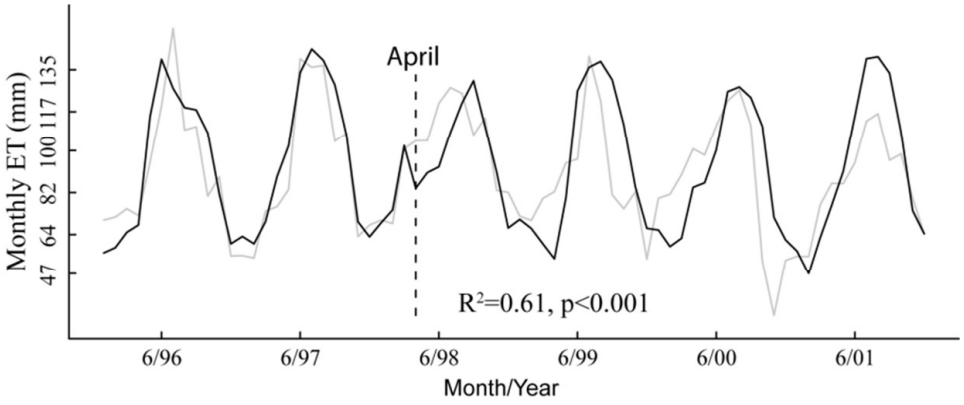

Fig. 4. Comparison between LH-simulated (black line) to observed (gray line) monthly ET (German, 2000) over the years 1996–2001 in the Everglades of Florida (US).

HESSD
9, 1207–1249, 2012

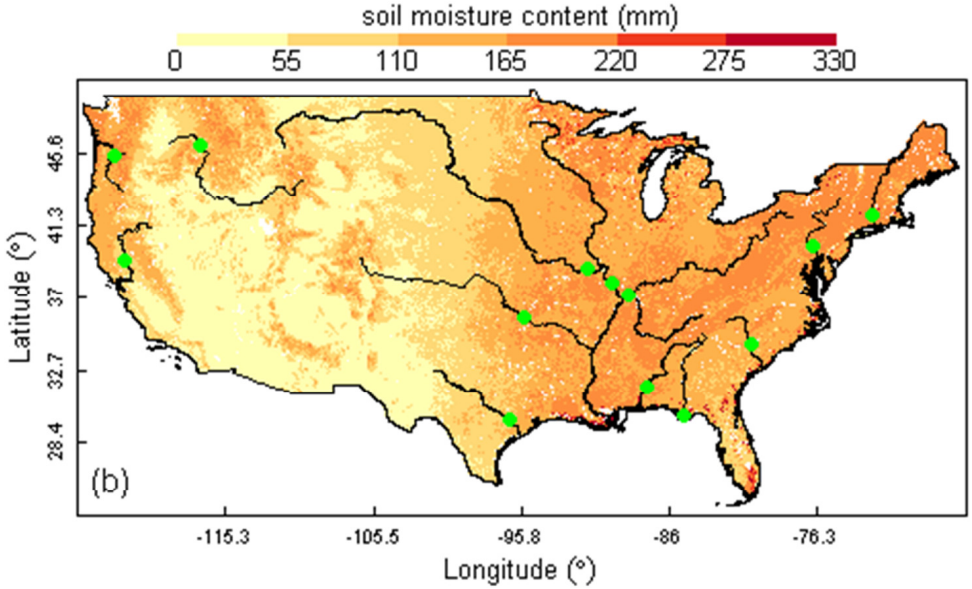

Fig. 5. The LH-simulated 26-yr' (1981–2006) average annual soil moisture in the top 50 cm of soil layers.

HESSD
9, 1207–1249, 2012

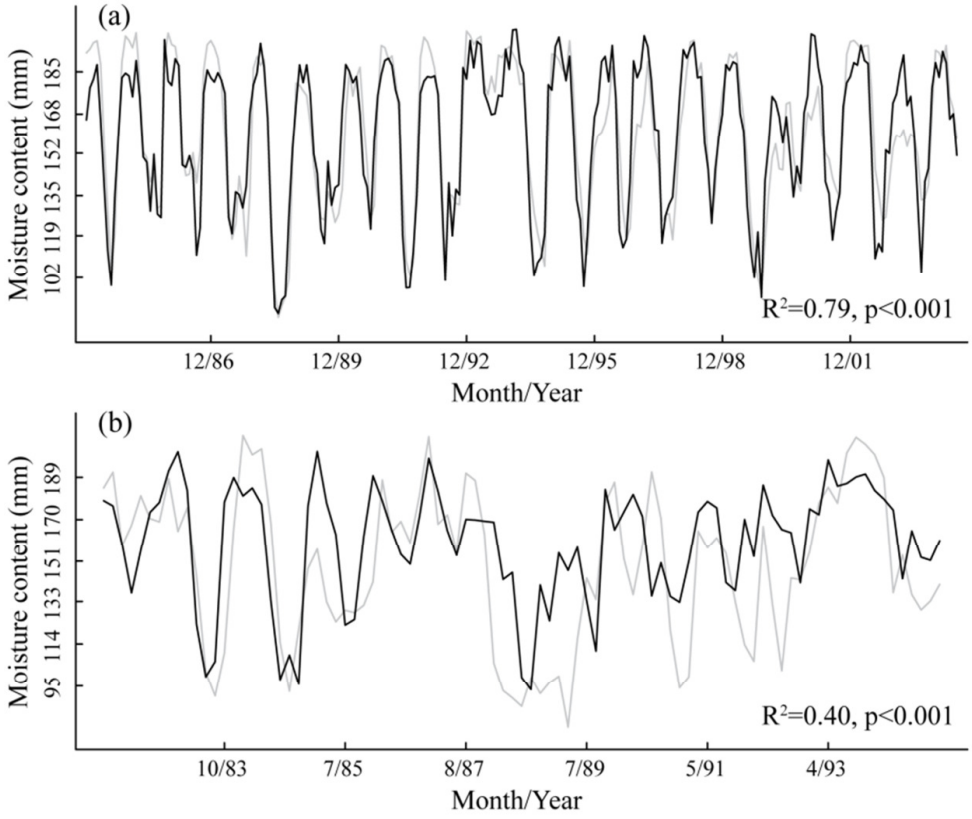

Fig. 6. Comparison between LH-simulated (black line) and observed (gray line) soil moisture in the top 50 cm of soil layers in **(a)** Illinois of the US over the years 1984–2004 (Hollinger et al., 1994) and **(b)** Iowa of the US over the years 1982 to 1994 (Entin, 1998; Entin et al., 1999). For Illinois soil moisture data, only half of years' (till June) data for the year 2004 are available. Measured soil moisture in Iowa is not available for some months and years but most are available between April and October.

HESSD
9, 1207–1249, 2012

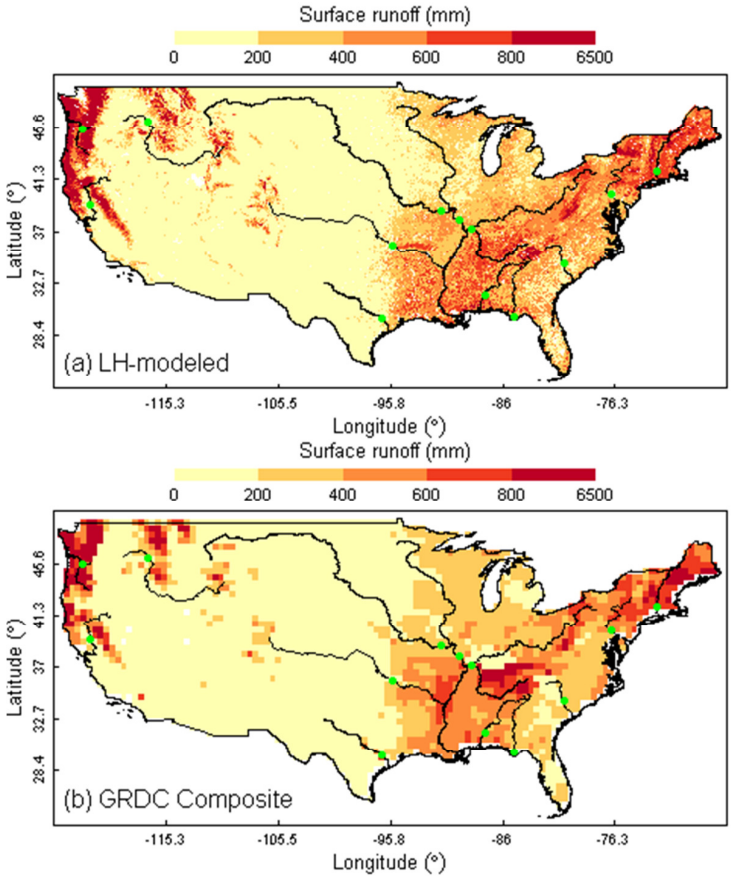

Fig. 7. (a) The LH-simulated annual surface runoff at 2.5 arc-min grid cells and **(b)** the GRDC composite annual runoff at 0.5 degree grid cells (Fekete et al., 2002) for the conterminous US.

HESSD
9, 1207–1249, 2012

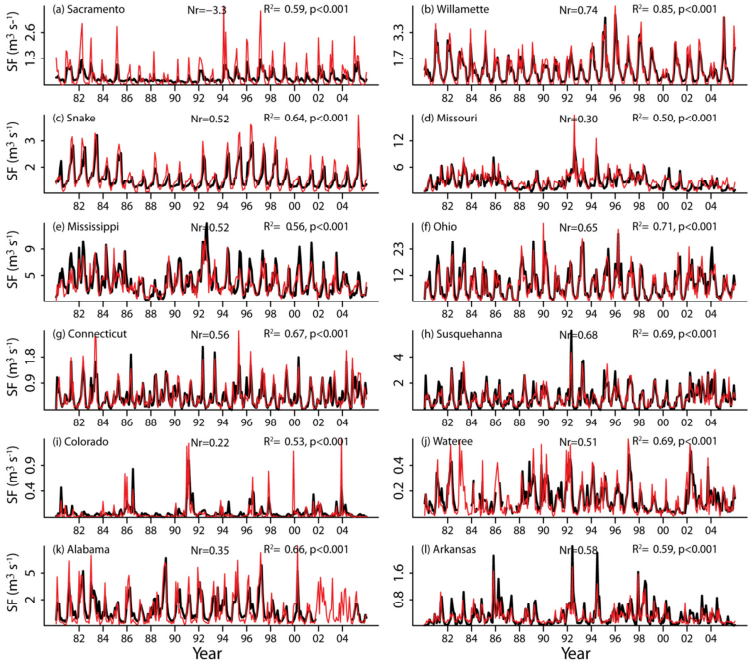

Fig. 8. Comparison between LH-simulated (red line) and the US Geological Survey monthly stream flow (SF) (black line) measured at 12 river gage stations. For plotting, the y-axis values are reduced by a factor of 10^3. Nr is the Nash-Sutcliffe coefficient.

HESSD
9, 1207–1249, 2012

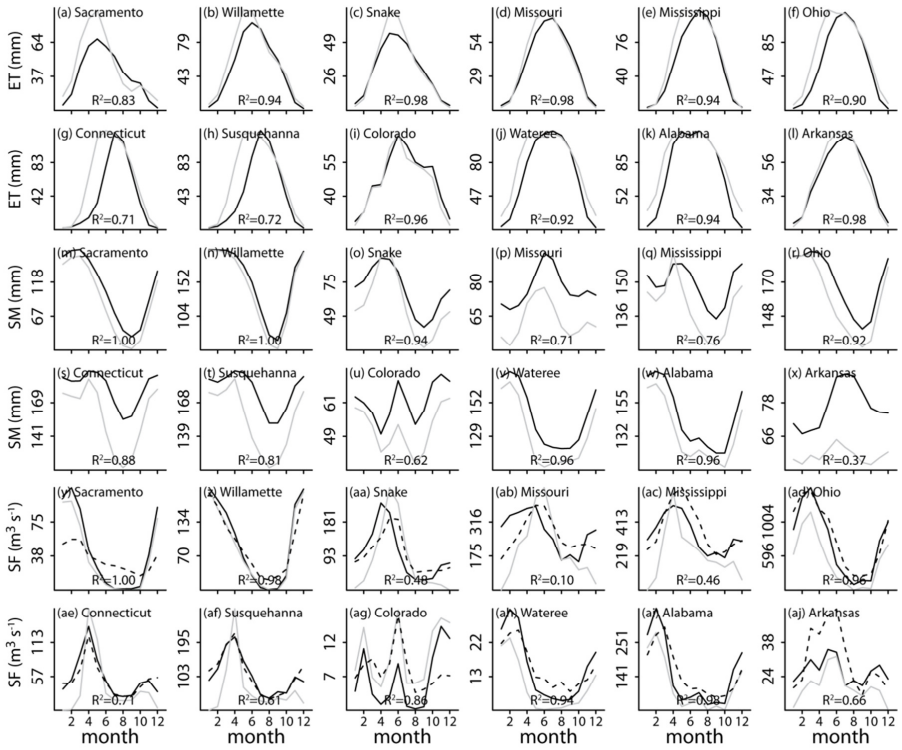

Fig. 9. Comparison between LH-(black line) and DGVM-simulated (gray line) **(a–l)** actual ET, (m-x) soil moisture (SM) and **(y–aj)** stream flow (SF) in 12 river watersheds. The black dashed line in **(y–aj)** is the USGS monthly stream flow from 12 combined gage stations. For plotting, the values of y-axis in **(y–aj)** are reduced by a factor of 10.

HESSD
9, 1207–1249, 2012